Chapter 3
Analysis and Interpretation of Interval and Count Variability in Neural Spike Trains

Martin Paul Nawrot

Abstract   Understanding the nature and origin of neural variability at the level of single neurons and neural networks is fundamental to our understanding of how neural systems can reliably process information. This chapter provides a starting point to the empirical analysis and interpretation of the variability of single neuron spike trains. In the first part, we cover a number of practical issues of measuring the inter-spike interval variability with the coefficient of variation (CV) and the trial-by-trial count variability with the Fano factor (FF), including the estimation bias for finite observations, the measurement from rate-modulated spike trains, and the time-resolved analysis of variability dynamics. In the second part, we specifically explore the effect of serial interval correlation in nonrenewal spike trains and the impact of slow fluctuations of neural activity on the relation of interval and count variability in stochastic models and in in vivo recordings from cortical neurons. Finally, we discuss how we can interpret the empirical results with respect to potential neuron-intrinsic and neuron-extrinsic sources of single neuron output variability.

3.1 Introduction

In the living animal, neural signals fluctuate on various temporal and spatial scales. Across experimental repetitions, neural responses may vary considerably in microscopic and macroscopic signals, both in invertebrate and vertebrate brains. Understanding how nervous systems ensure reliable function under the variable and seemingly noisy in vivo conditions is a key issue in computational systems neuroscience that is of fundamental importance for theories on sensory coding, learning and memory, and behavioral control.

M.P. Nawrot (✉)
Neuroinformatics and Theoretical Neuroscience, Institute of Biology, Freie Universität Berlin, Königin Luise Straße 1-3, 14195 Berlin, Germany
e-mail: martin.nawrot@fu-berlin.de
url: http://www.biologie.fu-berlin.de/neuroinformatik

1

PDF-OUTPUT

In this chapter, we introduce methods to analyze two aspects of neural output variability. The variance of inter-spike intervals reflects intra-trial variability on a relatively fast time scale of tens to hundreds of milliseconds. In contrast, the variance of the number of spikes counted during repeated experimental observations reflects a variability on a comparably slow time scale of seconds or even minutes. On theoretical grounds, interval and count statistics are fundamentally related. We will thus place a special focus on the coanalysis of both aspects, and we suggest ways to interpret their empirical relation in the light of stochastic models. The present chapter emphasizes practical issues that are relevant for the analysis of experimental data. The Appendix provides reference to a number of Matlab tools for point process simulation and spike train analysis which are publicly available with the FIND toolbox (Meier et al. 2008). Additional course material including example data sets is made available at the portal site of the German Neuroinformatics Node (http:www.g-node.org).

3.2 The Analysis of Inter-Spike Interval Variability

3.2.1 The Coefficient of Variation and Bias of Estimation

Definition 1 We consider the empiric observation of a series of spike events within a finite interval $(a, b]$ with $a < b$ and duration $T = b - a$. We assume a finite number of spike events N within $(a, b]$. We denote the spike times as $a < t_1 < t_2 < \cdots < t_N \leq b$ and define the $N - 1$ inter-spike intervals as $X_1, X_2, \ldots, X_{N-1}$, where $X_i = t_{i+1} - t_i$. Repeated and independent observations j result in an ensemble of k independent spike trains, each with a spike count N^j.

Practically, we obtain repeated independent measurements of action potentials either during repeated experimental trials, the time-frame of which is defined by the experimental protocol (e.g., in fixed temporal relation to a sensory stimulus presentation). Repeated observations may also be obtained through segmentation of a continuous spike train (e.g., recorded during sleep or under spontaneous conditions) into subsequent, nonoverlapping observation windows of equal length. In this section we assume the repeated observation of a spiking process that has a constant spike rate, and we assume that the constant firing rate is identical in each trial.

The empirical distribution of inter-spike intervals, its mean, variance, and higher moments generally depend on the length T of the observation window. Suppose that we empirically sample intervals X that were drawn from a fix interval distribution $f(x)$ within a finite observation window of length T as in Fig. 3.1A, where the observation window is expressed in multiples of the mean inter-spike interval (we will call this the operational time axis). Evidently, we can only observe intervals X that are shorter than the observation window T, and thus the empirical interval distribution is $\hat{f}(x) = 0$ for $x > T$ (cf. Fig. 3.1B). For all intervals $x \in (0, T]$, the likelihood of their observation is proportional to $T - x$, which leads to the following expression for the empiric distribution
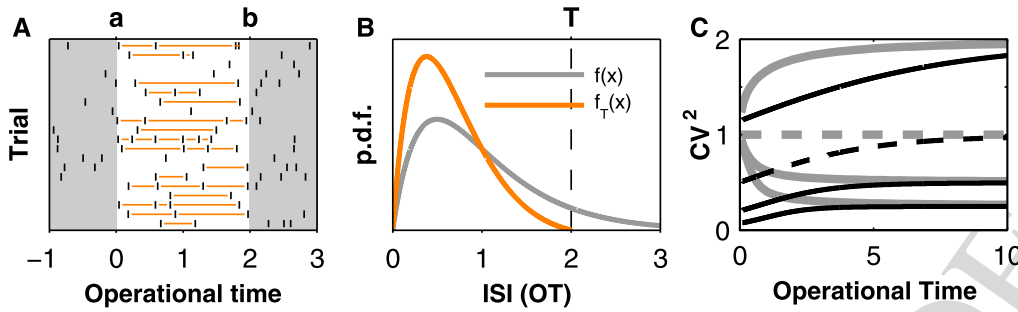
Fig. 3.1 Bias of CV estimator for a finite observation window. (**A**) Independent empiric observations (trials) of a gamma renewal process within the finite observation window $(0, 2]$ in operational time results in an empiric sample of inter-spike intervals X (*orange*). Intervals $X > T'$ cannot be observed; long intervals are more likely to span across one or both interval limits than short ones. (**B**) Gamma distribution $f(x)$ of order $\alpha = 2$ (*gray*) and distribution $\hat{f}(x)$ restricted to intervals $X \leq T' = 2$ (*orange*, (3.1), normalized to unit area). Mean and variance are clearly smaller for $\hat{f}(x)$ than for $f(x)$. (**C**) Dependence of the CV on the observation window. Shown is the expectation value for the empiric squared coefficient of variation CV^2 (*black*) and the Fano factor (*gray*; cf. 3.3.1) in dependence on the interval T' in operational time for gamma processes of different order $\alpha = 0.5, 1, 2, 4$ (from *top* to *bottom*). *Dashed lines* correspond to the Poisson process. For increasing T' the empiric CV^2 and the empiric FF approach $\mathsf{CV}_\infty^2 = 1/\alpha$

$$\hat{f}(x) = \begin{cases} \eta^{-1}(T - x) f(x) & \text{for } x \in [0, T], \\ 0 & \text{otherwise,} \end{cases} \tag{3.1}$$

where

$$\eta = \int_0^T (T - s) f(s) \, ds$$

normalizes the distribution to unit area. Thus, long intervals ($X \lesssim T$) are less frequently observed than short ones ($X \ll T$), a statistical effect also known as right censoring (Wiener 2003). This becomes intuitively clear when we consider that long intervals are likely to span across the left or right limit of our observation window such that, e.g., $t_i < a < t_{i+1}$. On the contrary, multiple small intervals may fit into one single observation (cf. Fig. 3.1A).

Definition 2 We define the empiric coefficient of variation for a set of inter-spike intervals as the standard deviation of interval lengths divided by the mean interval length

$$\mathsf{CV} = \frac{\mathsf{SD}[X]}{\mathsf{E}[X]}. \tag{3.2}$$

In the case of repeated independent observations (trials) j we have two options for computing the CV. The standard procedure is to compute the CV across the complete set of intervals pooled from all observations. Alternatively, we may first compute the individual CV^j for each trial separately and in a second step calculate the mean $\overline{\mathsf{CV}} = \frac{1}{k} \sum \mathsf{CV}^j$ across trials. Under stationary conditions where the generating stochastic process has a constant rate which is identical in all trials it follows that $\mathsf{CV} = \overline{\mathsf{CV}}$, on expectation.

139 Right censoring introduces a systematic error to the empirical estimation of the
140 coefficient of variation (Nawrot et al. 2008). For a unimodal interval distribution
141 the empirical CV underestimates the theoretical value CV_∞ that is derived from the
142 full distribution. To explore this effect in more detail we calculated the empirical
143 $CV(T')$ for the widely used model of the gamma interval distribution (see Appendix)
144 as a function of the observation time. In Fig. 3.1C we explore this dependence for
145 the *squared* coefficient of variation because it directly relates to the Fano factor
146 (see Subsect. 3.3.1). We find that the empiric CV^2 drops with decreasing observation
147 time. Conversely, with increasing observation time, the empiric CV^2 approaches the
148 theoretical CV_∞^2. The dashed line refers to the special case of the Poisson process
149 with $\alpha = 1$. Note, that we expressed observation time $T' = T/E[X]$ in multiples
150 of the mean inter-spike interval $E[X]$ (operational time), which gives results that
151 are independent of the actual firing rate. In practice, we may produce calibration
152 curves similar to those in Fig. 3.1C from experimental data to explore this bias
153 behavior in a given set of data. Elsewhere, we estimated that for regular spiking
154 cortical neurons, observation intervals that comprise about 5–10 ISIs are practically
155 of sufficient length to avoid a strong bias (Nawrot et al. 2008).

156

157

158 Due to the *finite length T* of the observation window, one cannot sam-
159 ple the full interval distribution $f(x)$ that is generally defined on $\mathbb{R}_+$. This
160 introduces a *bias of estimation for the empiric* CV which generally leads to
161 the *under*estimation of the theoretic CV_∞ (Fig. 3.1). Practical consequences:
162 1. Use long observation windows, i.e., clearly longer than the average ISI
163 $(T \gg E[X])$. 2. If short observation windows are necessary, e.g., to uncover
164 fast variability dynamics (see Fig. 3.2D), use a fixed window size in opera-
165 tional time to ensure a *constant* bias across repeated measurements.

166

167

168

3.2.2 Analysis of Rate-Modulated Spike Trains

170

171 The CV measures the dispersion of the interval distribution. It characterizes the ir-
172 regularity of spike trains and allows one to quantify the stochastic nature of the
173 observed spiking process. However, the CV is a useful measure only if the spike
174 rate is constant over time and if the variation of intervals is of stochastic nature such
175 as in the case of the gamma renewal process illustrated in Fig. 3.1. Whenever a
176 neuron modulates its output firing rate, e.g., in response to a sensory stimulus, then
177 this rate modulation strongly influences the empiric interval distribution. Any rate
178 modulations that are slow compared to the mean ISI will increase the dispersion of
179 the empiric interval distribution and thus lead to an increased CV which no longer
180 reflects the stochastic nature of the spiking process alone (see Fig. 3.2A).
181 Here, we describe one possible strategy to overcome this problem which requires
182 two additional steps of analysis as demonstrated in Fig. 3.2. First, one obtains an es-
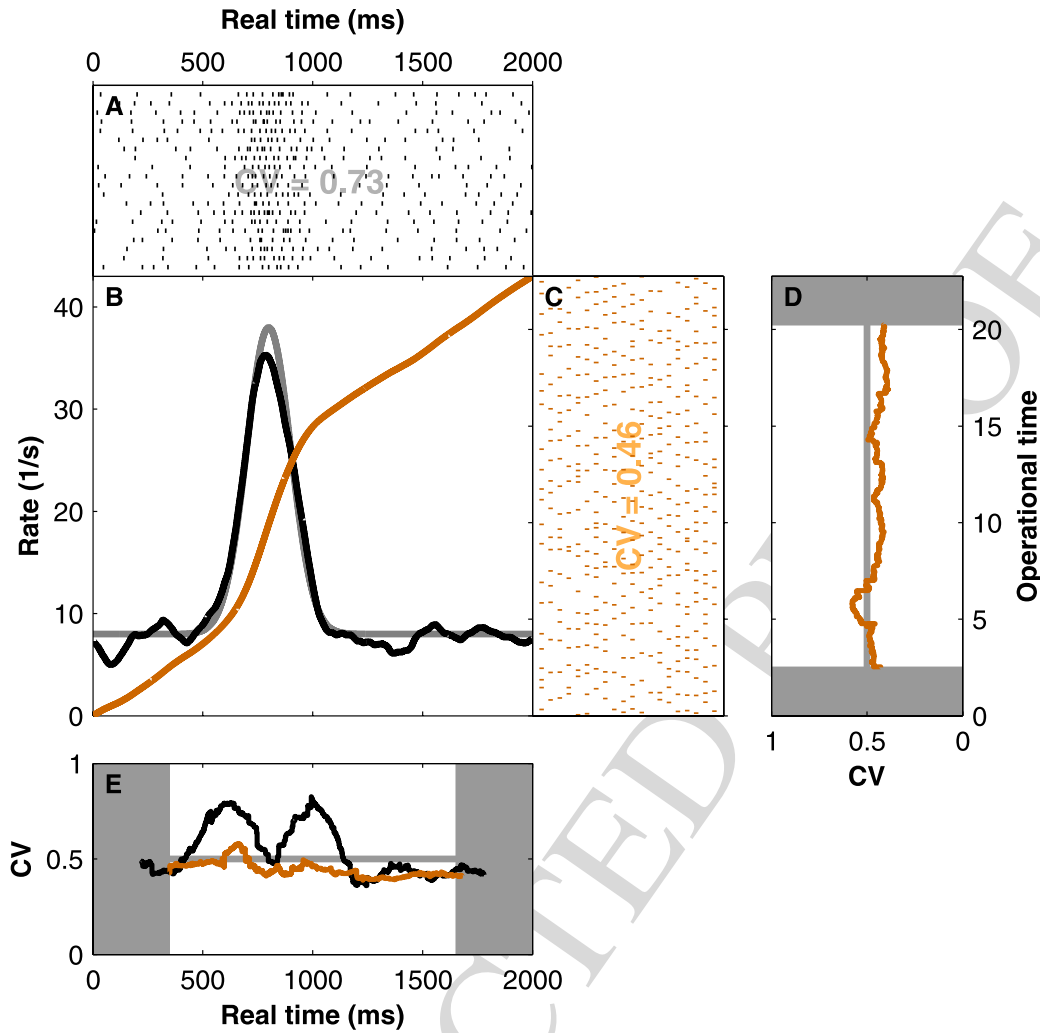183 timate $\hat{\lambda}(t)$ of the time-varying firing rate on the basis of repeated measurements.
184

Fig. 3.2 Estimation of interval variability in operational time. (**A**) Repeated observations of a rate-modulated gamma process with order $\alpha = 4$. We expect for the gamma renewal process $CV_\infty = 1/\sqrt{\alpha} = 0.5$. The empiric estimate $CV = 0.73$ is artificially increased due to the changing rate. (**B**) Kernel estimate of the time-varying firing rate $\hat{\lambda}(t)$ (*black*) from $N = 20$ spike trains in **A** (triangle kernel, $\sigma_k = 45$ ms) and integrated rate function $\Lambda(t)$ (*maroon*). The *gray function* depicts the original intensity used to simulate the spike trains in **A**. (**C**) Demodulated spike trains in operational time. Each single spike time in **A** was transformed according to $t_i' = \Lambda(t_i)$. In operational time the empiric estimate $CV = 0.46$ agrees well with the expectation $CV_\infty = 0.5$. (**D**) Time-resolved estimate of the CV in operational time. Window width is $T' = 5$. (**E**) Time-resolved CV as in **D** back-transformed to experimental time (*maroon*). The time-resolved CV estimated from the original spike trains in **A** (*black*) is modulated due to the changes in firing rate

Second, one transforms the experimental time axis to the so-called operational time axis such that the firing rate modulation is compensated (time warping). In operational time we then proceed with estimating the CV.

3.2.2.1 Step 1. Estimation of the Rate Function

Obtaining a reasonably good estimate of the rate function is crucial. Here, we use the method of linear kernel convolution (Nawrot et al. 1999; Shimazaki and Shinomoto

2009; Parzen 1962) with a fixed kernel function. After choosing a kernel shape which has little influence on the quality of the estimate, one has to fix the kernel width which determines the time resolution of the rate estimate. In the example of Fig. 3.2, we first pooled the spike trains from all observations (trials) and then estimated the trial-averaged rate function. To this end, we chose a symmetric kernel of triangular shape. To obtain an estimate for the optimal kernel width σ_k (defined as the standard deviation of the normalized kernel function) on the basis of the empirical data, we applied a heuristic method outlined elsewhere (Nawrot et al. 1999). Recently, Shimazaki and Shinomoto (2009) formalized this optimization of the kernel width for fixed and variable width kernels using a Bayesian approach on the basis of a specific model assumption for the generating point process. For fixed width kernels, this approach is outlined in detail in Chap. 2 of this book.

3.2.2.2 Step 2. Demodulation and Analysis in Operational Time

Based on the estimated firing rate $\lambda(t)$, we define the time transformation (Reich et al. 1998; Brown et al. 2002; Nawrot et al. 2008)

$$t' = \Lambda(t) = \int_0^t \lambda(s)\,ds, \tag{3.3}$$

according to the integrated rate function for all spike events t_i^j. We call t' the operational time because on this new time axis the empirical spiking process has constant unit rate. Figure 3.2B shows the integral $\Lambda(t)$ (maroon) of the empiric rate function $\lambda(t)$ (black). The transformed spike trains depicted in Fig. 3.2C do not display any overt rate modulation and result in an empiric estimate $\mathsf{CV} = 0.46$, which is close to the theoretic $\mathsf{CV}_\infty = 0.5$ of the underlying gamma process that was used for simulation.

> Transformation of spike times from the experimental time axis to the *operational time axis* according to the integrated rate function can eliminate rate fluctuations in the spike train. In a next step, this allows us to obtain an empiric estimate of the CV in operational time. This method requires a reliable estimate of the time-varying rate function (Fig. 3.2).

3.2.2.3 Time-Resolved Analysis of the CV

It is now straightforward to analyze the $\mathsf{CV}(t')$ as a function of operational time using a sliding window approach. The window width T' defines the time resolution of this analysis, and we are faced with a trade-off between short windows that ensure a good time resolution of our analysis and large windows that reduce the variance and the bias of estimation (see Subsect. 3.2.1). In Fig. 3.2D, we estimated $\mathsf{CV}(t')$ within a window of length $T' = 5$, i.e., the window size is 5 times the average

277 interval. We find no significant variation with a mean of $\langle \mathsf{CV}(t') \rangle = 0.45$, a faithful
278 representation of the underlying gamma process used for simulation in Fig. 3.2A. In
279 a final step we may use the inverse time transformation of (3.2) (Meier et al. 2008;
280 Nawrot et al. 2008) to represent our time-resolved estimate $\mathsf{CV}(t')$ in experimental
281 time $\mathsf{CV}(t)$ (see Fig. 3.2E). Note that the support points at which the measured
282 values $\mathsf{CV}(t)$ are represented are not equidistant in experimental time.

3.2.2.4 Alternative Methods

286 There are several alternative parametric and nonparametric methods to estimate in-
287 terval variability from rate-modulated spiking activity and in a time-resolved man-
288 ner. A number of nonparametric so-called *local measures* have been proposed that
289 estimate normalized interval variability locally in time. The common idea behind
290 these approaches is that a temporally confined estimate will largely ignore rate mod-
291 ulations that are comparatively slow. At each step in time, local measures are based
292 on rather small data samples and are thus inherently noisy—i.e., they express a
293 large variance of estimation—and they are in general subject to estimation biases.
294 Estimation variance may be decreased by temporal averaging over local estimates.
295 Here, I briefly outline two local measures. A simple yet efficient method for es-
296 timating the local CV from repeated trials has been introduced by Benda (2002).
297 At any given point in time t, this method computes the empiric CV from all in-
298 tervals in all trials that contain t, i.e., for which $t_i < t < t_{i+1}$. Evidently, shorter
299 intervals are less likely to be observed than longer ones. This introduces an esti-
300 mation bias with respect to the CV_∞ which is opposed to the one we described
301 in Subsect. 3.2.1, and which can be compensated (Nawrot and Benda 2006). Rate
302 fluctuations on a time scale that are longer than the average ISI will have little in-
303 fluence on this measure. It is, however, sensitive to across-trial nonstationarities of
304 the rate. The "classical" local measure termed C_{V2} was introduced in 1996 by Holt
305 et al. (1996). It simply computes the coefficient of variation for each successive pair
306 of intervals (X_i, X_{i+1}), i.e., it normalizes the variance across two successive inter-
307 vals by their mean and thus becomes insensitive to across-trial nonstationarities and
308 largely ignores rate modulations that are slower than twice the average ISI. Other
309 local measures are mostly variants thereof, and each has been designed under a cer-
310 tain optimization constraint. The robustness of these measures is typically increased
311 by averaging across trials and across time. An in-depth review and calibration of
312 the C_{V2} and three other local measures (Shinomoto et al. 2005; Davies et al. 2006;
313 Miura et al. 2006) was recently published by Ponce-Alvarez et al. (2009).

314 In competition to nonparametric local measures, a few parametric methods of
315 estimating the firing irregularity have been proposed. They assume a specific un-
316 derlying model (e.g., a nonhomogeneous Poisson process) and estimate a single or
317 several model parameters from the empiric spike train. Recently, Shimokawa and
318 Shinomoto (2009) introduced an elegant method for which they assume a gamma
319 process with time-varying intensity (firing rate) $\lambda(t)$ and time-varying regularity (or-
320 der of the gamma process) $\alpha(t)$. Using a Bayesian approach, the proposed method
321 allows us to estimate both $\lambda(t)$ and $\alpha(t)$ from a given set of empirical data.

3.3 The Combined Analysis of Interval and Count Variability

In the case of a mathematically defined point process model, its interval and count statistics are uniquely determined and inherently related (see Appendix). To characterize an unknown neural spiking process on the basis of experimental observations, it is therefore useful to coanalyze interval *and* count statistics, and their specific relation. This can help to choose a particular stochastic model (or a class of models) that adequately describes the experimentally observed process.

3.3.1 Fano Factor and Bias of Estimation

The Fano factor is a well-established measure of count variability and has been repeatedly used to quantify spike train variability (for review, see Nawrot et al. 2008).

Definition 3 The empiric Fano factor FF is defined as the ratio of the variance and the mean of the spike count N^j as measured within an observation interval of length T during repeated observations j:

$$\mathsf{FF} = \frac{Var[N^j]}{\mathsf{E}[N^j]}. \tag{3.4}$$

The distribution of spike count across repeated observations and thus the mean and variance of this distribution generally depend on the length T of the observation window. This introduces an estimation bias for the empiric FF with respect to the limit value $\mathsf{FF}_\infty = \lim_{T \to \infty} \mathsf{FF}$ which can be derived analytically from the definition of the process. In Fig. 3.1C we demonstrate how the Fano factor depends on the observation window $T' = T/\mathsf{E}[X]$ for gamma processes of different order α. With increasing observation time T', the FF estimates approach the limit values FF_∞. As for the CV, an observation window of length $T' = 5$–10 seems practically sufficient to avoid a strong bias if the observed process is more regular than the Poisson process ($\alpha \geq 1$), e.g., in regular spiking cortical neurons (Nawrot et al. 2008). For decreasing observation times $T' \to 0$, the Fano factor approaches unity. This can be easily understood as an approximation of the Bernoulli process for which in each small interval we observe either 1 spike with probability p or 0 spikes with probability $1 - p$. As $T' \to 0$, the variance $p(1 - p)$ of the Bernoulli distribution approaches the mean p (Teich et al. 1997).

The *finite length T* of the observation window introduces a *bias of estimation for the empiric FF* (Fig. 3.1C). As $T' \to 0$, the Fano factor approaches unity. Practical consequences as in Subsect. 3.2.1: 1. Use long observation windows, and 2. If short observation intervals are necessary, use a fix window size in operational time to ensure a *constant* bias.
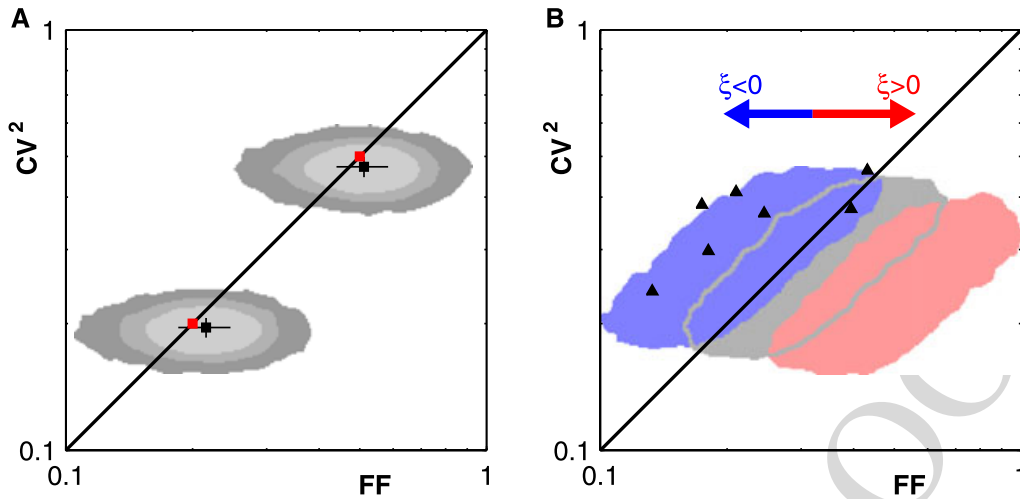
Fig. 3.3 Count variability (FF) versus interval variability (CV^2). (**A**) Variance of estimator and residual bias effect. The renewal prediction $FF_\infty = CV^2_\infty$ is depicted by the *black diagonal*. *Grey shadings* represent 90% confidence regions for numeric ensemble simulation of gamma processes of order $\alpha = 2$ ($CV^2_\infty = 0.5$) and $\alpha = 5$ ($CV^2_\infty = 0.2$). *Grey colors* indicate number of trials ($N = 20, 50, 100$, from *dark* to *light gray*). The observation time comprised $T' = 10$ intervals on expectation. Each confidence region was computed from 10,000 ensembles as follows. A 2D Gaussian filter produced a smooth 2D histogram of all log-transformed value pairs. After sorting all histogram entries starting with the largest entry, their cumulative sum was computed. All indices up to the index for which the 90% quantile was reached define the 2D confidence region. The *black squares* and *lines* depict average and standard deviation for $n = 100$ trials. The *red squares* indicate expectation values. (**B**) The effect of serial interval correlation on interval and count variability. *Colored shadings* represent the 90% confidence regions from 10,000 numeric ensemble simulations (50 trials, $T' = 10$) of the autoregressive process with marginal log-normal interval distribution (see text). The *blue* (*red*) *region* shows the effect of a negative (positive) serial interval correlation with respective parameter $\beta = -0.3$ ($\beta = 0.3$); *gray region* is computed from the interval-shuffled spike trains which do not exhibit serial correlations. *Black triangles* reproduce the empiric results obtained from 7 cortical cells (Nawrot et al. 2007). Data courtesy of Clemens Boucsein, University of Freiburg, Germany

3.3.2 Fano Factor vs. Squared Coefficient of Variation

For the class of renewal point processes, the expectation values of FF and CV^2 are simply related by

$$FF_\infty = CV^2_\infty. \tag{3.5}$$

Renewal processes are widely used as models for neural spiking. As a starting point for our analysis of experimental data, we may therefore formulate the renewal prediction (3.5) as the null-hypothesis. Any deviation from this null-hypothesis may then trigger further analysis.

A direct way of jointly visualizing the empiric relation of interval and count variability is to plot FF against CV^2 in a scatter diagram as demonstrated in Figs. 3.3 and 3.4. Individual empirical estimates of FF and CV^2 are computed from a finite number of samples and are, therefore, subject to statistical errors that is expressed in the variance of estimation (Nawrot et al. 2008). Repeated measurements will

thus lead to values that scatter around the theoretic expectation value. Figure 3.3A demonstrates the effect of a limited sample size in numeric simulations of the gamma renewal process with order parameters $\alpha = 2$ and $\alpha = 5$ and corresponding expectation values $CV^2_\infty = FF_\infty = 1/\alpha$. We chose different numbers of trials $n = 20, 50, 100$ and constructed the 90% confidence region from 10,000 independent simulations, depicted as gray shadings. The empirical sample size of intervals and counts scales linearly with the number of trials. Consequently, reducing the number of trials increases the variance of estimation for both, FF (horizontal) and CV^2 (vertical). The number of intervals additionally scales with T' and, thus, reducing observation time will increase the variance of the CV^2 estimator (not shown; Nawrot et al. 2008).

In practice, residual estimation biases due to the experimentally limited observation time T for CV^2 (see Subsect. 3.2.1) and FF (see Subsect. 3.3.1) may affect their empirical relation. As a consequence, in Fig. 3.3A the average empiric values for $T' = 10$ (black squares) of the Fano factor is larger, and the average empiric value of the CV^2 is smaller than the expectation values indicated by red squares.

> For any (stationary) renewal point process, the relation of Fano factor and coefficient of variation is given by $FF_\infty = CV^2_\infty$. For the special case of the Poisson process, it holds that $FF = CV^2_\infty = 1$.

3.3.3 The Effect of Serial Interval Correlation

Renewal processes represent the most prominent class of stochastic models for neural spiking. Yet, serial correlations of inter-spike intervals have been observed experimentally in various systems including neocortical cells (for review, see Farkhooi et al. 2009). For stationary point processes in equilibrium with serially correlated inter-event intervals, the following equality holds (McFadden 1962; Cox and Lewis 1966):

$$\lim_{T \to \infty} FF = CV^2_\infty (1 + 2\xi) \quad \text{with } \xi = \sum_{i=1}^{\infty} \xi_i, \tag{3.6}$$

where ξ_i denotes the ith-order linear correlation coefficient, i.e., the expected linear correlation for all pairs of intervals (ISI_k, ISI_{k+i}) that are separated by $i - 1$ intermediate intervals. If all correlation coefficients vanish, we obtain the renewal statistics where $FF_\infty = CV^2_\infty$. Overall negative serial correlation $\xi < 0$ will result in a Fano factor that is smaller than the CV^2, while a positive correlation $\xi > 0$ leads to an increased count variability.

We demonstrate this effect in numerical simulations of a simple autoregressive model as outlined in (Farkhooi et al. 2009) (see Appendix). The intervals X of this model are log-normal distributed. The serial correlation of intervals is controlled

by an additional correlation parameter β. Correlations are short ranged, i.e., the linear correlation coefficients ξ_i quickly diminish with increasing serial correlation order i (Farkhooi et al. 2009). In Fig. 3.3B, we consider two cases: (i) *negative* serial correlation of ISIs ($\xi < 0$, blue), and (ii) *positive* correlation ($\xi > 0$, red). Both are compared to the corresponding renewal process ($\xi = 0$, gray). In each case we simulated 10,000 spike train ensembles of 50 trials, and each ensemble represents the repeated measurement of one neuron with a single estimate for CV^2 and FF. For each neuron, we adjusted the model parameters to obtain a specific value of the squared coefficient of variation in the range $CV^2_\infty \in [0.2, 0.5]$. This covers the empirically relevant range for regular spiking neocortical neurons under stationary conditions (e.g., Nawrot et al. 2007; Nawrot et al. 2008). From all 10,000 simulated samples we numerically constructed the confidence region which covers 90% of the measurements. As theoretically predicted, the negative serial correlations reduce the Fano factor, in this case by about 30%, while positive correlations increase the Fano factor by about 60%.

To compare the modeling results with experimental findings, we reanalyzed intracellular recordings from rat somatosensory cortex of the anesthetized rat (Nawrot et al. 2007). 7 of 8 regular spiking cortical cells expressed short-ranged negative interval correlations with $\xi \approx -0.2$ leading to a count variability reduced by 30% (black triangles in Fig. 3.3B).

> *Negative* serial interval correlations ($\xi < 0$) in a stationary point process realization lead to a *reduced* count variance as compared to the count variance of a renewal process with the same interval distribution, and thus $FF < CV^2$. *Positive* serial interval correlations ($\xi > 0$) lead to an *increased* count variance, and thus $FF > CV^2$; see (3.6) and Fig. 3.3B.

3.3.4 The Effect of Nonstationarity

In the typical experimental situation, we make repeated observations in time (trial design). This allows us to perform statistical analyses on the trial ensemble, e.g., estimating the trial-averaged firing rate or the variance of the spike count across trials. By doing so, we make the implicit assumption that the observed spiking process is stationary in time and across trials (Knoblauch and Palm 2005; Nawrot et al. 2008). However, this assumption is often violated in neural systems. In this section we explore the influence of a particular type of nonstationarity: we assume slow modulations of the firing rate on time scales of seconds or even minutes. In the living animal, such modulations are likely to occur for various reasons (see Sect. 3.4).

3.3.4.1 Slow Activity Fluctuations Introduce Across-Trial Nonstationarity

To model slow fluctuations of the firing rate, we use the following approach. In a first step we generate a time-dependent intensity $\phi(t)$ using a moving average process with log-normal distributed noise (see Appendix). The intensity (or rate) fluctuates about the mean of $r = 1$ Hz on a slow time scale $\tau' = 20$ in operational time (e.g., equivalent to a rate of 10 Hz and $\tau = 2$ s in experimental time). In the next step we generate a realization of a rate-modulated gamma process with intensity $\phi(t)$ and order parameter $\alpha = 2$ and with a total duration of 500 expected spikes in operational time. In a final step we divide this spike train into $n = 50$ observations (or trials) of length $T' = 10$ and analyze interval and count variability. Again, we compute confidence regions for FF vs. CV^2 in the scatter diagram of Fig. 3.4A.

The Fano factor is boosted by the additional nonstationarity (green shadings) and can reach very high values that are up to 20 times larger than in the stationary case (gray shading). This effect can be easily understood. The expectation value for the spike count varies from trial to trial as the process intensity modulates on long time scales and thus across trials. This has a dramatic effect on the distribution and variance of the spike count. The CV^2 is only slightly increased (light green shading), and the effect dominates in ensembles that also show high count variability. The general explanation for the increased CV^2 is simple: shorter intervals in trials with higher intensity and longer intervals in trials of lower intensity will lead to an additional dispersion of the interval distribution. This effect can be avoided. In Subsect. 3.2.1 we introduced an alternative way of estimating the $\overline{CV}^2$ by estimating the CV_i in each individual trial and subsequent averaging. This procedure normalizes per trial and thus is not susceptible to across-trial nonstationarities. In Fig. 3.4A the dark green shading indicates the corresponding confidence region. In summary, the FF is strongly increased, while the distribution of the $\overline{CV}^2$ with mean 0.37 is similar to that of the control with mean 0.38.

We compare the simulation results to a set of in vivo single unit recordings from the primary motor cortex of a monkey (*Macaca mulatta*) that performed a delayed center-out reaching task (Rickert et al. 2009). We analyzed interval and count variability during the first 900 ms of the 1-s delay period. At the start of this period, the monkey had received a directional cue but was not allowed to move his arm until the GO signal appeared at the end of the delay period. Many neurons showed a task-related activation profile that was tuned for the specific target cue. We therefore estimated the trial-averaged firing rate and performed the analysis in operational time (see Subsect. 3.2.2). The results are shown in Fig. 3.4B. The Fano factor assumes high values with a mean of FF $= 1.87$ (median 1.39), while the values of the CV^2 are considerably lower with average $CV^2 = 0.76$ (median 0.70). The shape of the 90% confidence region compares to that of the numeric simulations in Fig. 3.4A. Two additional factors will likely lead to an overestimation of the empiric CV^2 in the present data. First, we may assume that the activity is not stationary across trials due to slow modulations, as in our model simulations. As a consequence, the resulting estimate of the task related rate profile from the trial-averaged spike trains does not properly reflect the single-trial rate profile. Second, we deal with another type
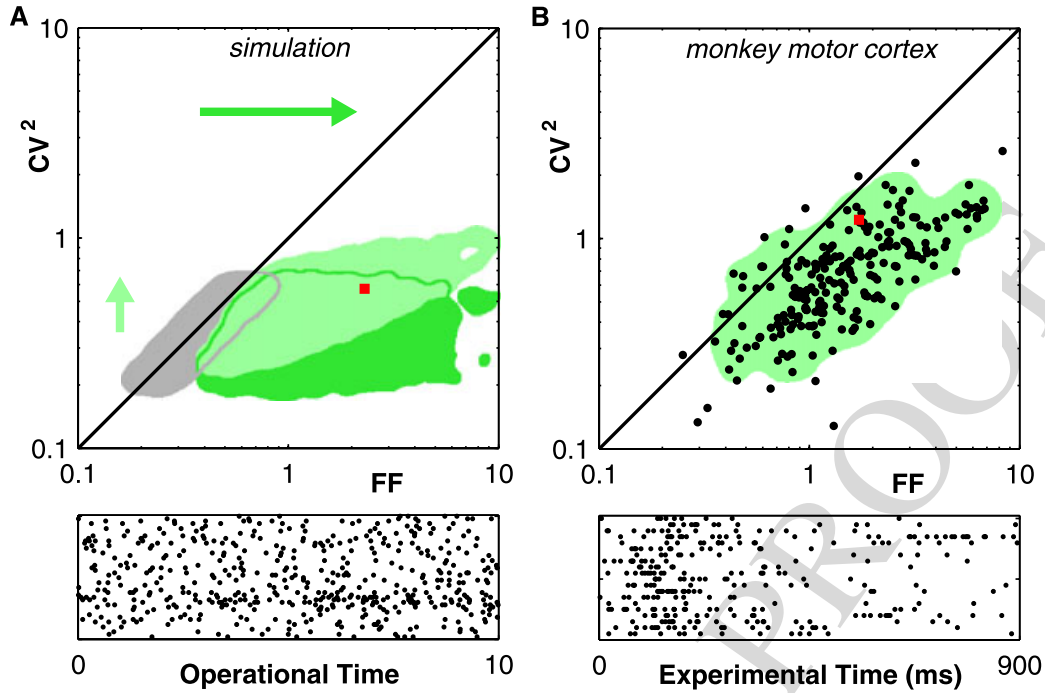
Fig. 3.4 Slow rate modulations can boost count variance. (**A**) Simulation. The *gray shading* represents the confidence interval for gamma processes with $\alpha \in [2, 5]$. The *green shadings* demonstrate the effect of slow modulations of the process intensity (MA log-normal noise; $\sigma = 200$, $\tau' = 20$). The FF is strongly increased. The empiric CV^2 (*light green*) was estimated by pooling intervals from all trials. The $\overline{CV}^2$ (*dark green*) was estimated in each trial separately and then averaged. *Bottom panel* shows spike raster for one ensemble (*red square*). (**B**) Experiment. In vivo estimates from 56 motor cortical single units, each recorded in 6 directions (see text). The FF strongly exceeds the CV^2. The CV^2 was estimated from intervals pooled across trials. For each ensemble the number of trials was ≥ 15 (to limit the variance) and the observation window comprised $T' \geq 10$ intervals (to avoid a strong bias). This included a total of 223 samples. *Bottom panel* shows one example (*red square*). Modified from (Nawrot et al. 2001; Nawrot 2003). Data courtesy of Alexa Riehle, CNRS, Marseille, France

of variability, namely the trial-by-trial variation of the response onset time (Nawrot et al. 2003). This further impairs the trial-averaged estimate of the rate profile. Both factors will lead to an imperfect demodulation of the single-trial spike trains and, thus, to an increased dispersion of the inter-spike interval distribution and an increased empiric CV^2. An in-depth analysis of interval and count variability for this data set and a second monkey is provided in (Nawrot 2003). A time-resolved analysis of variability for this monkey (monkey 1) is provided in (Rickert et al. 2009).

In the model of slow rate fluctuations, we introduced a single time scale τ' for the temporal modulation. How does this time scale interact with the length T' of the empiric observation interval? In Fig. 3.5A, B the Fano-time curve $FF(T')$ displays a nonmonotonic behavior resulting from two independent factors. For small observation times $T' \leq E[X]$, the bias effect dominates, and the FF tends to unity as $T' \to 0$. With increasing $T' > E[X]$, the slow intensity fluctuations cause a strong increase in count variance. As the positive serial interval correlations introduced by the rate fluctuation vanish for large correlation lags $i \gg \tau'$ (Fig. 3.5C), the FF saturates for large $T' \gg \tau'$ (Fig. 3.5B) because the spike count averages across the
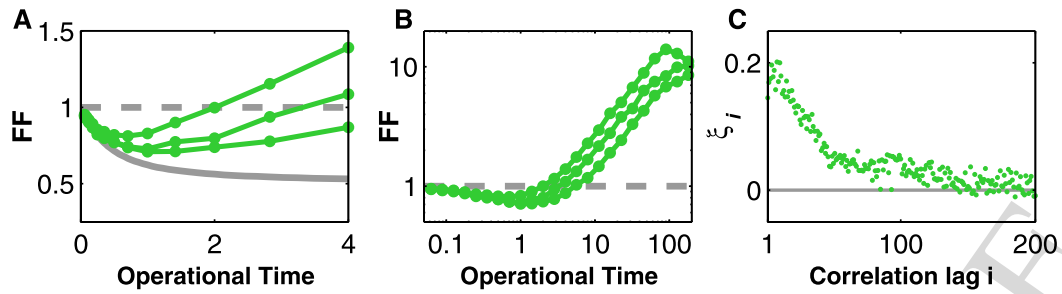
Fig. 3.5 Effect of slow rate modulations on the Fano-time curve and serial interval correlation. (**A**) $FF(T')$ estimated from three individual realizations of a rate-modulated gamma process of order $\alpha = 2$. The process intensity $\phi(t)$ was modulated according to an MA process with log-normal noise ($\sigma = 200$, $\tau' = 20$). The *gray curve* represents the expectation value for the stationary gamma process. (**B**) For large observation intervals $T' \gg \tau'$, the Fano factor saturates. (**C**) Serial interval correlation coefficients diminish only for large serial correlation lags $i \gg \tau'$

stochastic fluctuations within the observation interval. Importantly, the trial-by-trial variability assumes a *minimum* for observation times $T' \approx \mathsf{E}[X]$, which is even more pronounced for a nonrenewal process with short-lived negative serial interval correlation (not shown; see Subsect. 3.3.3).

3.3.4.2 Task-Related Variability Dynamics

In a next step we extended the previous model for slow-rate modulation by adding a task-related response profile $\psi(t)$ during repeated trials that represents task-related activation of a neuron (or neural ensemble), e.g., in response to a stimulus. We model $\psi(t)$ with a Gaussian profile as in Subsect. 3.2.2. Now we have the situation that the same intensity profile repeats identically in each trial and adds to a fluctuating background $\phi(t)$. How does this affect the time-resolved variability? Figure 3.6 shows the result: The time-resolved Fano factor (blue curve) expresses a task-related dynamics. It is high during the initial phase of the trial before the response is triggered at $t = 0$ and again at the end of the trial. During the response, the FF strongly decreases and almost reaches the expected value for a stationary process with $FF = 1/\alpha = 0.5$. This modulation can be easily understood: Whenever the firing rate is dominated by the task-related component ψ, the relative trial-by-trial fluctuations of the point process intensity, and thus of the empiric Fano factor, are minimal. Conversely, at times when the task-related component ψ is essentially zero, the spike count variability is dominated by the trial-to-trial variations due to the fluctuating intensity $\phi(t)$. The trial-based estimate of the $\overline{CV^2}$ (dark green curve in Fig. 3.6D) does not show any apparent modulation. It correctly signifies the "true" stochasticity of the underlying gamma process except for a small bias that underestimates the expected value CV_∞^2 (see Subsect. 3.2.1). The ratio of FF/CV^2 in Fig. 3.6F combines both analyses and reveals dynamic deviations from the renewal hypothesis for which $FF = CV^2$.
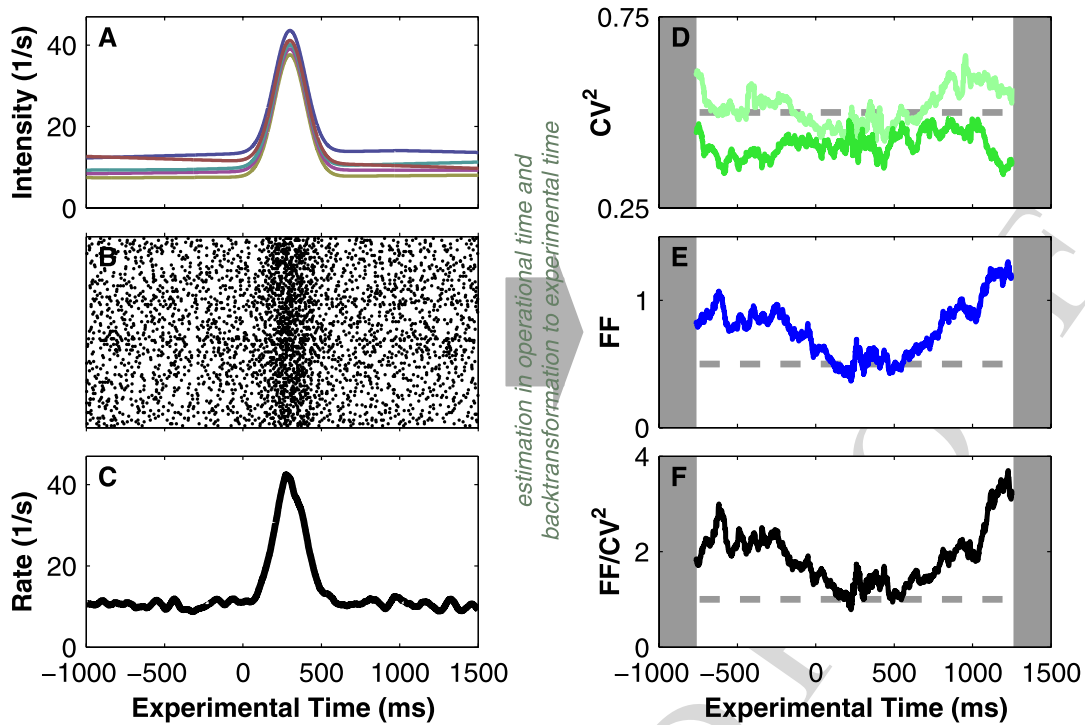
Fig. 3.6 Temporal modulation of spike count variability. (**A**) Five individual single trial intensities resulting from the superposition of the slow fluctuating background rate $\phi(t)$ and the task-related Gaussian modulation $\psi(t)$ (width $\sigma = 100$ ms, amplitude 30/s). (**B**) Spike raster from rate-modulated gamma process ($\alpha = 2$) realizations during 100 trials. (**C**) Kernel estimate of firing rate. (**D**) The time-resolved CV^2 (*light green*) is slightly modulated. The $\overline{CV^2}$ (*dark green*) expresses an expected residual bias. (**E**) Time-resolved FF. (**F**) The ratio of $FF/\overline{CV^2}$ combines both analyses. Renewal prediction $FF_\infty = CV^2_\infty$ is indicated by the dashed line. Length of observation interval in **D**–**F** was $T' = 5$

Slow modulations of the output firing rate can be modeled by a nonstationary point process with time-varying intensity $\phi(t)$ and large time constant of modulation $\tau \gg E[X]$. Such a modulation introduces a positive serial interval correlation ($\xi > 0$) and can *strongly increase the count variance*. The CV^2 is less sensitive to the nonstationarity. As a result, we observe that $FF > CV^2$ (see Fig. 3.4A). When this model is combined with a task-related intensity profile $\psi(t)$ which is identical in each trial, we observe a task-related modulation of the $FF(t)$ (see Fig. 3.6).

3.4 Interpretations

3.4.1 Components of Single Neuron Variability

We may coarsely distinguish two components of single-neuron output variability (DeWeese and Zador 2004). The first component is attributable to neuron-*intrinsic*

sources such as synaptic failures and variability of synaptic event amplitude (e.g., DeWeese and Zador 2004; Nawrot et al. 2009; Zador 1998), noise caused by dendritic integration (e.g., Nawrot et al. 2009; Ariav et al. 2003; Shoham et al. 2005), and the reliability of spike initiation (e.g., Mainen and Sejnowski 1995; Nowak et al. 1997). The second, neuron-*extrinsic* component results from the spatial and temporal statistics of the synaptic input, i.e., the spiking statistics of the presynaptic excitatory, inhibitory, and neuromodulatory networks. Biological neurons are nonlinear, complex input–output devices that translate synaptic input into an output comprising a sequence of action potentials. When we analyze a neuron's output, we cannot distinguish between the different sources that caused the observed variability. Also, the concept of an "intensity" that we use in the framework of stochastic point process theory and that we like to interpret as "underlying rate" of neural firing has no physical equivalent in biological neurons. Therefore, we must base our interpretations on additional numerical studies of biophysical neuron models and experimental studies that focus on basic neural mechanisms in reduced preparations, which allow for highly controlled experimental conditions.

3.4.2 Serial Interval Correlations

Negative serial correlations have been reported for various neuron types in invertebrate and vertebrate systems (for review, see Farkhooi et al. 2009). These correlations are short-ranged, typically extending over only a few intervals, and they are of intermediate strength (e.g., $\xi \approx -0.2$ for cortical neurons) which results in a considerable reduction of the Fano factor of up to 50%. A plausible physiological explanation for this phenomenon are neuron-*intrinsic* mechanisms of spike frequency adaptation (SFA) (Benda and Herz 2003), which can introduce negative interval correlations in the output spike train when the neuron is in a steady state (i.e., for constant output rate), a result that has been established in various types of biophysical single neuron models (e.g., Wang 1998; Prescott and Sejnowski 2008; Muller et al. 2007). The reduction of the Fano factor implies that SFA neurons have an improved signal-to-noise ratio which increases the coding capacity of a rate code on slow time scales. On fast time scales, i.e., for very short observation windows, however, the Fano factor tends to unity (see Subsect. 3.3.1). In the frequency domain this results in a reduction of the low frequency noise (noise shaping; Chacron et al. 2001, 2005; Lindner et al. 2005; Chacron et al. 2007).

Systematic reports of negative serial correlations in experimental data are rare, in particular, in central brain structures such as the neocortex or the central insect brain. We briefly discuss two factors that may impair their empiric observation. First, serial correlation analysis assumes stationarity of the spike train. Any modulation of the firing rate will introduce positive serial correlations, which may conceal the negative correlations and increase the Fano factor (see Subsect. 3.3.4). The second issue is of technical nature. At extracellular electrodes we measure spikes that stem from

multiple neurons. Subsequent spike sorting—to some extent—represent the activity of multiple neurons. From surrogate data we estimated that only 10–15% falsely assigned spikes can impair the detection of realistic negative serial correlations in recordings that comprise $\sim 1{,}000$ spikes (unpublished observation).

In the context of cross-correlation analysis of two (or more) simultaneously recorded neurons, renewal models are typically used to calculate the expected joint count distribution under the assumption that the neurons' activity is independent. Serial interval correlations affect the joint count distribution, and the renewal statistics may thus not be appropriate to test for deviations from independent spiking in SFA neurons (Grün et al. 2008).

3.4.3 Nonstationary Conditions in the Living Brain

There have been frequent reports on a large trial-by-trial variability in in vivo single-unit recordings, notably in the mammalian cortex where, with few exceptions, large average values of the Fano factor ($\mathsf{FF} \geq 1$) have been measured (e.g., Shadlen and Newsome 1998; for review, see Nawrot et al. 2008). This has lead to the dogma that the activity of cortical neurons is well characterized by Poisson statistics, which has subsequently become a benchmark for cortical network models. However, the large variability in vivo is contrasted by a series of in vitro studies that have quantified the output variability of pyramidal neurons for stationary input conditions. They used intracellular injection of currents generated by stochastic trains of excitatory and inhibitory synaptic inputs. It showed that the interval and count variability is in the range of $\mathsf{CV}^2 \approx \mathsf{FF} \in [0.1, 0.8]$, depending mostly on the relative fractions of excitation and inhibition (for review, see Nawrot et al. 2008). Negative serial interval correlations may further reduce the count variance such that $\mathsf{FF} < \mathsf{CV}^2$ (Fig. 3.3B; Nawrot et al. 2007). From these studies we may conclude that—for stationary input conditions—cortical neurons are more regular and less variable than the Poisson process.

What could be the reason for the discrepancy between the in vivo and in vitro results? One possibility is that in the living brain, stationary input conditions do not exist for neurons that are embedded in a recurrent and permanently active network. Local networks may be exposed to global changes of their activation state, e.g., due to homeostatic regulation, changes in the general state of arousal, plasticity, adaptation, etc., and they may be subject to top–down influences such as attentional modulation.

The simple stochastic model outlined in Subsect. 3.3.4 generates a random fluctuation of the firing intensity that underlies the stochastic production of spike events. We found that slow modulations of the intensity on time scales $\tau \gg \mathsf{E}[X]$ can strongly increase the count variance across independent observations, leading to large values of $\mathsf{FF} \gg 1$ as observed in vivo. The more important result, however, is expressed in the relation of count and interval variability. The CV^2 was only

slightly increased so that $FF \gg CV^2$, indicative of positive serial interval correlations due to the slow-rate modulations. This is what we also observed in the single-unit recordings from M1 in the behaving monkey (Fig. 3.4B; Nawrot et al. 2001; Nawrot 2003). These results suggest nonstationary input conditions in vivo, and they may indicate that the large in vivo variability does not characterize the stochastic nature of the individual neuron. Experimental studies (Nowak et al. 1997; Carandini 2004; Nawrot 2003) suggest that even mild fluctuations in the neuron's input are sufficient to cause a strong variability in the neuron's output. This is explained by the nonlinear transfer function of synaptic input drive and output firing rate. Mechanistically, such modulation of the presynaptic network input may be achieved by various means, e.g., through unbalancing of (presynaptic) excitatory and inhibitory networks, or through neuromodulatory regulation.

A number of theoretical models have investigated the effect of long-ranged temporal correlations in the driving noise of biophysical model neurons. These studies established the result of positive serial interval correlations in the output spike train and of the nonmonotonic behavior of the Fano-time curve (Chacron et al. 2001; Middleton et al. 2003; Schwalger and Schimansky-Geier 2008; Farkhooi et al. 2009). The strong increase of the Fano factor with increasing observation window, and in some cases also the characteristic of a nonmonotonic Fano-time dependence, has been reported in several experimental studies, e.g., in the cat striate (Teich et al. 1996) and in the monkey motor cortex (Nawrot 2003), in the LGN (Teich et al. 1997), in the retina (Teich et al. 1997), and most pronounced in the electrosensory afferents of the weakly electric fish (Ratnam and Nelson 2000). The fact that experimental Fano-time curves can express a minimum for a certain range of observation times may indicate that there exists an optimal temporal scale for information processing in these systems.

In Fig. 3.6A we added to the spontaneous intensity fluctuation $\phi(t)$ a task-related phasic component $\psi(t)$, which repeats identically in each trial. As a direct consequence, we observe a task-related modulation of the Fano factor. Indeed, this behavior has been repeatedly observed in motor cortical single-unit activity (Nawrot et al. 2001, 2003; Nawrot 2003; Churchland et al. 2006; Nawrot et al. 2008; Rickert et al. 2009) and, more recently, also in other cortical areas (Churchland et al. 2010). Thus, we may hypothesize that individual neurons or neural populations are specifically recruited for a computational task, e.g., the processing of a sensory stimulus, through a task-specific and dynamic input that overrides the background input, which represents ongoing activity and/or global changes of the network activation state.

Appendix

3.4.4 Matlab Tools for Simulation and Analysis

The following functions are available online in the FIND open source Matlab toolbox (Meier et al. 2008); http://find.bccn.uni-freiburg.de/.

makeKernel	builds simple kernel functions of predefined shape and normalized temporal width (Nawrot et al. 1999; Meier et al. 2008); used in Subsect. 3.2.2.
optimizeKernelWidth	estimates the optimal kernel width from spike train data according to a heuristic method (Nawrot et al. 1999; Meier et al. 2008); used in Subsect. 3.2.2.
sskernel	optimizes kernel width from spike train data according to the method by Shimazaki and Shinomoto (Shimazaki and Shinomoto 2009).
unWarpTime	demodulation of point or counting process according to a monotonic warp function. For details, see (Nawrot et al. 2008; Meier et al. 2008).
warpTime	inverse modulation of point or counting process.
gamprc/simulateGamma	simulates constant rate/rate-modulated gamma process using time rescaling.
arlogn/simSCP	simulates autoregressive log-normal point processes; used in Sect. 3.2. For details, see (Farkhooi et al. 2009).

3.4.5 Point Process Models

Chapter 1 of this book provides a formal introduction to stochastic point process theory, covering a number of issues that have been addressed in the present chapter. Chapter 16 deals in more detail with the simulation of stochastic point processes.

For any point process, *interval and count statistics are related*. Define the kth-order interval as $\tau_k = \sum_{i=1}^{k} X_i$. For an ordinary process, $\tau_k \leq t \iff N_{[0,t)} \geq k$. The distribution of τ_k relates to the distribution of event count N by

$$P\{\tau_k \leq t\} = P\{N_{[0,t)} \geq k\}.$$

The class of *renewal point processes* is widely used for the simulation of neural spiking. The renewal process is defined as a process for which all inter-event intervals are independent and identically distributed. Thus, we can define a particular renewal process by specifying its interval distribution. For nonbursting neurons, there are a number of distributions that have been repeatedly used, in particular, the (centralized) gamma distribution which includes the special case of the Poisson process, the log-normal distribution, and the inverse Gaussian distribution.

The interval distribution of the (centralized) *gamma process* is defined as

$$f_{\alpha,\rho}(x) = \begin{cases} \frac{1}{\Gamma(\alpha)}\,\rho(\rho x)^{\alpha-1}e^{-\rho x}, & x \geq 0, \\ 0, & x < 0, \end{cases}$$

where Γ denotes the gamma function, and $\alpha > 0$ and $\rho > 0$ are its two parameters. The mean interval is α/ρ, and the variance is α/ρ^2. For $\alpha = 1$, we obtain the Poisson process. For $\alpha > 1$, the gamma process is more regular and, for $0 < \alpha < 1$, more irregular than the Poisson process.

We used an *autoregressive model* to generate serially correlated interval series. A generalization of this model is described in detail elsewhere (Farkhooi et al. 2009). Assume that a series of random variables $Y_s = \beta Y_{s-1} + \varepsilon_s$, where ε_s is assumed to be normally distributed with mean μ and variance σ_N^2. β describes the serial dependence of the series Y_s. Then, the series

$$X_s = \exp(Y_s) = \exp(\beta Y_{s-1} + \varepsilon_s)$$

is asymptotically log-normal distributed. For parameterization according to definitions of $\mathsf{E}[Y]$ and CV, we used the following relations:

$$\sigma_N = \sqrt{\log(\mathsf{CV}^2 + 1)(1 - \beta^2)},$$
$$\mu = \log(\mathsf{E}[Y]) * (1 - \beta) - \sigma^2(1 - \beta)/(2(1 - \beta^2)).$$

In Subsect. 3.3.4, we simulated a *moving-average noise process* to generate a modulated rate function $\phi(t)$. To this end we drew random noise samples from a log-normal distribution with mean 1 (corresponding to unit rate) and standard deviation $\sigma = 200$ with a time resolution of 0.01 (operational time). In a second step we convolved the noise with a symmetric kernel of triangular shape and standard deviation $\sigma_k = 20$ (operational time). The resulting rate function fluctuates on a time scale that is 20 times larger than the mean interval.

References

Ariav G, Polsky A, Schiller J (2003) Submillisecond precision of the input–output transformation function mediated by fast sodium dendritic spikes in basal dendrites of CA1 pyramidal neurons. J Neurosci 23:7750–7758

Benda J (2002) Single neuron dynamics-models linking theory and experiment. Ph.D. thesis, Humboldt Universität zu Berlin. Ph.D. Dissertation

Benda J, Herz AVM (2003) A universal model for spike-frequency adaptation. Neural Comput 15(11):2523–2564. doi:10.1162/089976603322385063

Brown EN, Barbieri R, Ventura V, Kaas RE, Frank LM (2002) The time-rescaling theorem and its application to neural spike train data analysis. Neural Comput 14:325–346

Carandini M (2004) Amplification of trial-to-trial response variability by neurons in visual cortex. PLoS Biology 2(9):1483–1493

Chacron MJ, Lindner B, Longtin A (2007 Dec) Threshold fatigue and information transfer. J Comput Neurosci 23(3):301–311

Chacron MJ, Longtin A, Maler L (2001) Negative interspike interval correlations increase the neuronal capacity for encoding time-dependent stimuli. J Neurosci 21(14):5328–5343

Chacron MJ, Maler L, Bastian J (2005 May) Electroreceptor neuron dynamics shape information transmission. Nat Neurosci 8(5):673–678

Churchland M, Yu B, Cunningham J, Sugrue L, Cohen M, Corrado G, Newsome W, Clark A, Hosseini P, Scott B, Bradley D, Smith M, Kohn A, Movshon J, Armstrong K, Moore T, Chang S, Snyder L, Lisberger S, Priebe N, Finn I, Ferster D, Ryu S, Santhanam G, Sahani M, Shenoy K (2010) Stimulus onset quenches neural variability: a widespread cortical phenomenon. Nat Neurosci 13(3):369–378

Churchland MM, Yu BM, Ryu SI, Santhanam G, Shenoy KV (2006) Neural variability in premotor cortex provides a signature of motor preparation. J Neurosci 26(14):3697–3712

Cox DR, Lewis PAW (1966) The statistical analysis of series of events. Methuen's monographs on applied probability and statistics. Methuen, London

Davies RM, Gerstein GL, Baker SN (2006) Measurement of time-dependent changes in the irregularity of neural spiking. J Neurophysiol 96:906–918

DeWeese MR, Zador AM (2004) Shared and private variability in the auditory cortex. J Neurophysiol 92:1840–1855

Farkhooi F, Strube-Bloss M, Nawrot MP (2009) Serial correlation in neural spike trains: experimental evidence, stochastic modelling, and single neuron variability. Phys Rev E 79:021905

Grün S, Farkhooi F, Nawrot MP (2008) Significance of coincident spiking considering inter-spike interval variability and serial interval correlation. In: Frontiers comp neurosci conf abstr: neuroinformatics 2008. doi:10.3389/conf.neuro.11.2008.01.021

Holt GR, Softky WR, Koch C, Douglas RJ (1996) Comparison of discharge variability in vitro and in vivo in cat visual cortex neurons. J Neurophysiol 75(5):1806–1814

Knoblauch A, Palm G (2005) What is signal and what is noise in the brain? Biosystems 79:83–90

Lindner B, Chacron MJ, Longtin A (2005 Aug) Integrate-and-fire neurons with threshold noise: a tractable model of how interspike interval correlations affect neuronal signal transmission. Phys Rev E Stat Nonlin Soft Matter Phys 72(2 Pt 1):021911

Mainen ZF, Sejnowski TJ (1995) Reliability of spike timing in neocortical neurons. Science 268:1503–1506

McFadden J (1962) On the lengths of intervals in stationary point processes. J Roy Stat Soc B 24:364–382

Meier R, Egert U, Aertsen A, Nawrot MP (2008) Find – a unified framework for neural data analysis. Neural Networks 21:1085–1093. http://find.bccn.uni-freiburg.de/

Middleton JW, Chacron MJ, Lindner B, Longtin A (2003 Aug) Firing statistics of a neuron model driven by long-range correlated noise. Phys Rev E Stat Nonlin Soft Matter Phys 68(2 Pt 1):021920

Miura K, Okada M, Amari S (2006) Estimating spiking irregularities under changing environments. Neural Comput 18:2359–2386

Muller E, Buesing L, Schemmel J, Meier K (2007) Spike-frequency adapting neural ensembles: Beyond mean adaptation and renewal theories. Neural Comput 19(11):2958–3010

Nawrot M, Aertsen A, Rotter S (1999) Single-trial estimation of neuronal firing rates: from single-neuron spike trains to population activity. J Neurosci Meth 94:81–92

Nawrot M, Aertsen A, Rotter S (2003) Elimination of response latency variability in neuronal spike trains. Biol Cybern 5(88):321–334

Nawrot MP (2003) Ongoing activity in cortical networks: noise, variability and context. Ph.D. thesis, Faculty of Biology, Albert-Ludwigs-University Freiburg, Germany. URN: nbn:de:bsz:25-opus-73426. http://www.freidok.uni-freiburg.de/volltexte/7342/

Nawrot MP, Benda J (2006) Two methods for time-resolved inter-spike interval analysis. In: Berlin neuroforum abstr, p 62

Nawrot MP, Boucsein C, Rodriguez-Molina V, Aertsen A, Grün S, Rotter S (2007) Serial interval statistics of spontaneous activity in cortical neurons in vivo and in vitro. Neurocomputing 70:1717–1722

Nawrot MP, Boucsein C, Rodriguez Molina V, Riehle A, Aertsen A, Rotter S (2008) Measurement of variability dynamics in cortical spike trains. J Neurosci Meth 169:374–390

Nawrot MP, Rodriguez V, Heck D, Riehle A, Aertsen A, Rotter S (2001) Trial-by-trial variability of spike trains in vivo and in vitro. Soc Neurosci Abstr 27:64.9

Nawrot MP, Schnepel P, Aertsen A, Boucsein C (2009) Precisely timed signal transmission in neocortical networks with reliable intermediate-range projections. Frontiers Neural Circ 3:1. doi:103389/neurv.04.001.2009

Nowak LG, Sanchez-Vives MV, McCormick DA (1997) Influence of low and high frequency inputs on spike timing in visual cortical neurons. Cereb Cortex 7:487–501

Parzen E (1962) On estimation of a probability density function and mode. Ann Math Statist 33:1065–1076

Ponce-Alvarez A, Kilavik B, Riehle A (2009) Comparison of local measures of spike time irregularity and relating variability to firing rate in motor cortical neurons. J Comput Neurosci. doi:10.1007/s10827-009-0158-2

Prescott SA, Sejnowski TJ (2008) Spike-rate coding and spike-time coding are affected oppositely by different adaptation mechanisms. J Neurosci 28:13649–13661

Ratnam R, Nelson M (2000) Nonrenewal statistics of electrosensory afferent spike trains: implications for the detection of weak sensory signals. J Neurosci 20(17):6672–6683

Reich DS, Victor JD, Knight BW (1998) The power ratio and the interval map: Spiking models and extracellular recordings. J Neurosci 18:10090–10104

Rickert J, Riehle A, Aertsen A, Rotter S, Nawrot MP (2009) Dynamic encoding of movement direction in motor cortical neurons. J Neurosci 29:13870–13882

Schwalger T, Schimansky-Geier L (2008) Interspike interval statistics of a leaky integrate-and-fire neuron driven by Gaussian noise with large correlation times. Phys Rev E Stat Nonlin Soft Matter Phys 77(3 Pt 1):031914

Shadlen MN, Newsome WT (1998) The variable discharge of cortical neurons: Implications for connectivity, computation, and information coding. J Neurosci 18(10):3870–3896

Shimazaki H, Shinomoto S (2009) Kernel bandwidth optimization in spike rate estimation. J Comput Neurosci. doi:10.1007/s10827-009-0180-4

Shimokawa T, Shinomoto S (2009) Estimating instantaneous irregularity of neuronal firing. Neural Comput 21:1931–1951

Shinomoto S, Miura K, Koyama S (2005) A measure of local variation of inter-spike intervals. Biosystems 79:67–72

Shoham S, O'Connor DH, Sarkisov DV, Wang SSH (2005) Rapid neurotransmitter uncaging in spatially defined patterns. Nature Meth 2:837–843

Teich MC, Heneghan C, Lowen SB, Ozaki T, Kaplan E (1997) Fractal character of the neural spike train in the visual system of the cat. J Opt Soc Am A Opt Image Sci Vis 14(3):529–546

Teich MC, Turcott RG, Siegel RM (1996) Temporal correlation in cat striate-cortex neural spike trains. IEEE Eng Med Biol Mag 15(5):79–87

Wang XJ (1998) Calcium coding and adaptive temporal computation in cortical pyramidal neurons. J Neurophysiol 79:1549–1566

Wiener MC (2003) An adjustment of the time-rescaling method for application to short-trial spike train data. Neural Comput 15:2565–2576

Zador A (1998) Impact of synaptic unreliability on the information transmitted by spiking neurons. J Neurophysiol 79:1219–1229